IIETA International Information and Engineering Technology Association
Advancing the World of Information and Engineering

Mathematical Modelling of Engineering Problems
Vol. 12, No. 8, August, 2025, pp. 2650-2660
Journal homepage: http://iieta.org/journals/mmep

Impact of Equilibration Steps on Quantum Monte Carlo for the Spin-1/2 Heisenberg Model

Ali Akbar H. Ali*, Mohammad G. Merdan, Hayder M. Abdualjalil

Department of Physics, College of Science, University of Babylon, Babil 51001, Iraq

Corresponding Author Email: ali.shreib667@student.uobabylon.edu.iq

Copyright: ©2025 The authors. This article is published by IIETA and is licensed under the CC BY 4.0 license (http://creativecommons.org/licenses/by/4.0/).

https://doi.org/10.18280/mmep.120806

Received: 9 August 2024
Revised: 15 December 2024
Accepted: 26 December 2024
Available online: 31 August 2025

Keywords:
linear chain, Stochastic Series Expansion, spin-1/2 Heisenberg model, antiferromagnetic systems, quantum Monte Carlo, specific heat, ground state energy, computational efficiency, equilibration steps

ABSTRACT

This study delves into the pivotal role of equilibration Monte Carlo steps (i_{steps}) in the Stochastic Series Expansion method—a cutting-edge quantum Monte Carlo technique known for its precision in simulating low-dimensional quantum systems. The research focuses on how varying equilibration steps impact the accuracy and stability of ground state energy, sublattice magnetization, specific heat, and susceptibility results, by analyzing the effect of equilibration steps on these physical properties across different temperatures and lattice sizes. Our findings demonstrate that while ground state energy and sublattice magnetization achieve remarkable stability, susceptibility and specific heat present variabilities, especially at low temperatures. Ground state energy stabilizes after approximately 50 equilibration steps. However, excessive equilibration steps lead to unnecessary computational costs without further accuracy improvements. Furthermore, increasing the measurement steps significantly reduces error bars, enhancing reliability, as demonstrated by a 30% reduction in standard deviation with higher counts. Low temperatures exhibit greater variability in specific heat and susceptibility due to complex quantum effects.

1. INTRODUCTION

The spin-lattice model is a mathematical framework used to study interacting spins arranged on a lattice, representing quantum systems like magnets [1]. These models are described using Hamiltonians, which capture spin interactions and quantum properties and are often explored through analytical methods (e.g., Bethe ansatz) or numerical techniques (e.g., Monte Carlo) [2]. Spin lattice models are crucial for understanding quantum phenomena like phase transitions and entanglement. The Stochastic Series Expansion (SSE) method efficiently handles these models by directly sampling the partition function's power series, avoiding discretization errors and enabling precise simulations of thermodynamic properties [3, 4].

The SSE method is a very efficient quantum Monte Carlo (QMC) technique widely used in simulating quantum systems at finite temperatures [5-7]. This method is valuable in studying complex quantum phenomena, especially in low-dimensional and strongly correlated systems [8]. SSE leverages Taylor series expansion on the partition function of the system combined with nonlocal Monte Carlo updates [9], allowing direct sampling of the partition function expansion in powers of the Hamiltonian. This capability enables SSE to accurately simulate the thermodynamic properties of quantum spin systems, which is crucial in understanding quantum phase transitions and magnetic properties. This approach avoids the errors associated with time discretization [10].

An important factor in the development of QMC techniques has been Feynman's path integral formulation of quantum statistical mechanics [11]. World-line methods are frequently used to refer to techniques based on the path integral in imaginary time in the context of spin systems and related lattice models [12, 13]. The methods began by using an approximation discretization of imaginary time, known as the Suzuki-Trotter decomposition of the Boltzmann operator $e^{-\beta\hat{H}}$; β is the inverse dimensionless temperature. Such methods often introduce systematic errors due to discretization [14]; such errors arise because discrete jumps approximate the continuous dynamics of the system. This means that the true nature of quantum fluctuations is not fully captured. Additionally, Trotter-Suzuki Approximation Errors, a systematic error occurs because of splitting the exponential of a sum of operators into a product of exponentials [15, 16], each involving smaller time steps. This error decreases with the square of the time steps; however, achieving high-accuracy simulation requires smaller time steps, which increases the computational cost. SSE effectively avoids such errors by directly expanding the partition function in terms of a power series of the Hamiltonian operators with discretizing. Furthermore, SSE does not require Trotter-Suzuki approximations [10]. The progress in the QMC algorithm has mainly been made in two areas: (a) by removing the systematic error found in the Trotter decomposition and (b) by creating loop-cluster algorithms to enable efficient sampling inside the configuration space of quantum systems. SSE is a generalization of Handscomb's QMC scheme, which combines (a) and (b) with even more speedups for SSE's loop-cluster algorithms. Such speedups provide a shorter time for autocorrelation than other methods, enabling the studies of

larger system sizes [17, 18].

Monte Carlo steps play various critical roles in the SSE method. They ensure the accuracy of sampling configuration space and that the results represent the true equilibrium properties of the system. Monte Carlo steps bring the system into thermal equilibrium in the first phase of the simulation, allowing the system to reach a steady state where the sampled configurations represent the system's equilibrium distribution [19, 20].

Monte Carlo steps used in equilibration [21] are termed (i_{steps}) in this paper. Proper equilibration provides unbiased results when measurements are taken. Furthermore, each step of Monte Carlo simulation proposes an accept or reject of the new configuration of the system based on a probabilistic criterion; typically, Metropolis and other algorithms are used in this process. Efficient sampling ensures that all simulated configurations are considered according to their Boltzmann weights, accurately estimating physical quantities, such as energy, magnetization, and susceptibility. Monte Carlo steps are also used in diagonal and loop updates. The term used to refer to the Monte Carlo steps taken while measuring system properties is M_{steps} (i.e., measurements taken after the system has reached equilibrium). One bin represents the average of all individual results obtained at each M_{steps}.

This paper studies the impact of Monte Carlo steps used for equilibration on the computational cost, stability, and feasibility of SSE results for various properties, including ground state energy, sublattice magnetization, specific heat, and susceptibility for different lattice sizes and temperatures.

This work aims to investigate the impact of i_{steps} on the accuracy, stability, and computational efficiency of the SSE simulations, particularly for the 1D Heisenberg mode. The motivation stems from the crucial role equilibration plays in ensuring that Monte Carlo simulations correctly sample the equilibrium state of a quantum system. While significant progress has been made in understanding Monte Carlo methods and their applications, systematic studies quantifying the relationship between i_{steps}, physical observables, and computational costs remain limited.

The study commences with an overview of the foundational formulation of the SSE method, including the mathematical framework underpinning this approach. Subsequently, the results and discussion section present an analysis of the simulation outcomes, focusing on computational cost, magnetic properties of the system, and data convergence. The paper also provides a guide for researchers on selecting appropriate simulation parameters to ensure reliable results. The study's limitations are then outlined, followed by a concluding section summarizing the key findings of the research.

2. FORMULATION OF SSE

The spin-1/2 antiferromagnetic model is described by the Hamiltonian in terms of raising and lowering spin operators, such that [22, 23]:

$$\hat{H} = \frac{1}{2} J \sum_{\langle i,j \rangle} \left(\hat{S}_i^+ \hat{S}_j^- + \hat{S}_i^- \hat{S}_j^+ + 2\Delta \hat{S}_i^z \hat{S}_j^z \right) - h \sum_i \hat{S}_i^z, \tag{1}$$

where, J is the coupling constant, and it is positive for antiferromagnetic systems [24], $\langle i,j \rangle$ represents a pair of nearest-neighbor spin sites. S^+ and S^- are the raising and lowering spin operators, respectively. $\hat{S}^z$ denotes the spin operators in the Z direction. Δ and h are uniaxial anisotropy and external magnetic fields, respectively. The following Hamiltonian can represent the SSE method for this model:

$$\hat{H} = -J \sum_{b=1}^{N_b} \hat{H}_b \ (J > 0). \tag{2}$$

$N_b = dN$ is the number of bonds in a d-dimensional cubic lattice. We can further form two operators from the bond operator:

$$\hat{H}_b = \hat{H}_{1,b} - \hat{H}_{2,b}, \tag{3}$$

where, $\hat{H}_{1,b}$ and $\hat{H}_{2,b}$ are diagonal and off-diagonal operators;

$$\begin{aligned} \hat{H}_{1,b} &= c - \Delta \hat{S}_{i(b)} \hat{S}_{j(b)}^z + h_b \left[\hat{S}_{i(b)} + \hat{S}_{j(b)}^z \right] \\ \hat{H}_{2,b} &= \frac{1}{2} \left[\hat{S}_{i(b)}^+ \hat{S}_{j(b)}^- + \hat{S}_{i(b)}^- \hat{S}_{j(b)}^+ \right], \end{aligned} \tag{4}$$

$h_b \equiv h/(2dJ)$ is the magnetic field applied to a bond. To ensure that all elements of the $\hat{H}_{1,b}$ matrix are positive the constant c must be determined. i.e., $c \geq \Delta/4 + h_b$. c and c_0 represent:

$$c = c_0 + \epsilon, \ c_0 = \frac{\Delta}{4} + h_b, \tag{5}$$

where, $\epsilon \geq 0$. For the isotropic case, $c = \frac{1}{4}$ and $\epsilon = 0$.

The main focus of applying QMC to a quantum system is calculating the quantum mechanical thermal expectation value of an observable $\hat{A}$,

$$\langle \hat{A} \rangle = \frac{1}{Z} \mathrm{Tr}\{ \hat{A} e^{-\beta \hat{H}} \}, \tag{6}$$

where, Z is the partition function,

$$Z = \mathrm{Tr}\{ e^{-\beta \hat{H}} \}. \tag{7}$$

In SSE, the above equations are calculated using Taylor series expansion and making the traces as sums of diagonal matrix components in the basis $\{ |\alpha\rangle = |S_1^z, \dots, S_N^z\rangle \}$. The partition function can be formulated as [23]:

$$Z = \sum_\varphi \sum_{n=0}^{\infty} \sum_{S_n} \frac{(-1)^{n_2} \beta^n}{n!} \langle \varphi | \prod_{i=1}^{n} \hat{H}_{a_i,b_i} | \varphi \rangle, \tag{8}$$

where,

$$\begin{aligned} S_n &= [a_1, b_1][a_2, b_2] \dots [a_n, b_n], \\ a_i &\in \{1,2\}, b_i \in \{1, \dots, 2N\}. \end{aligned} \tag{9}$$

Is a sequence of index pairs defining the operator string $\prod_{i=1}^{n} \hat{H}_{a_i,b_i}$, and n_2 represents the total number of index pairs $[a_i, b_i]$, where, $a_i = 2(n = n_1 + n_2)$ and N represents the number of sites in the lattice equals $L \times 1$ for linear chain. Eq. (8) deviate from Handscomb's technique [25]. A scheme for importance sampling for terms in the partition function must be developed. The configuration $(\varphi, \hat{S}_n)$ determined by a basis state $|\varphi\rangle$ and operator sequence. $\hat{H}_{1,b}$ and $\hat{H}_2, b$ can act only on antiparallel spins at sites $i(b)$ and $j(b)$. Diagonal operator $\hat{H}_{1,b}$ keeps the spin state unchanged, while the off-diagonal operator flips the spin pair. The following equation denotes the propagated state:

$$|\varphi(p)\rangle = \prod_{i=1}^{p} \hat{H}_{a_i,b_i}|\varphi\rangle, |\varphi(0)\rangle = |\varphi\rangle. \quad (10)$$

$(\varphi, \hat{S}_n)$ must satisfy periodicity condition $|\varphi(n)\rangle = |\varphi(0)\rangle$ so that it can contribute in Eq. (8) For even numbers of spin sites in lattice, the total number of off-diagonal operators n_2 should be even, which makes all terms in Eq. (8) positive. Furthermore, this can be used as relative probabilities in the Monte Carlo importance sampling process. Taylor expansion could be truncated at some upper-bound l that is automatically chosen where the error is negligible.

The partition function can be represented by the weight of $(\varphi, \hat{S}_n)$ configuration as follows:

$$Z = \sum_{\varphi} \sum_{S_l} W(\varphi, S_l), \quad (11)$$

where, all non-zero matrix elements in Eq. (8) equal one, so the weight can be written as:

$$W(\varphi, S_l) = \left(\frac{\beta}{2}\right)^n \frac{(l-n)!}{l!}, \quad (12)$$

Here, n denotes expansion power of the configuration, i.e., represents the non-[0,0] operators of S_l.

A Monte Carlo Step (MC step) means performing a series of single-diagonal operator swaps at each point in S_l. Then, a series of off-diagonal updates on each bond will be performed. As a result of the constraints being localized in these updates, the number of operations (CPU time) per MC step increases proportionally with N and β.

3. RESULTS AND DISCUSSION

The simulation of 1D spin-1/2 antiferromagnetic system defined by the Heisenberg model using SSE was analyzed to explore the effect of i_{steps} on the system's physical properties, including ground state energy per spin (E_0/N), specific heat (C), sublattice magnetization $(\langle m^2 \rangle)$, and susceptibility (χ). The simulations were implemented in FORTRAN90, utilizing the Sandvik algorithm to perform the SSE calculations [26]. The computational work was executed on a personal computer equipped with an AMD Ryzen 7 3700X 8-Core Processor (3.60 GHz) and 16 GB of G. Skill Radiant 3600 MHz RAM, ensuring the capability to handle the significant computational demands of the study. We first present the computational cost for a range of temperatures and i_{steps}. Furthermore, the study investigates the stability of the simulation outcomes for different temperatures and multiple i_{steps} counts. Additionally, the same conditions but changing the steps were conducted to examine if the technique returned converged results and also for a range of temperatures. In this study, also we performed simulations on relatively large systems and low temperatures to examine the effectiveness of SSE on complex conditions.

3.1 Computational cost

This study investigates the impact of i_{steps} on processing time and found that they have a significant effect. It's clear that processing time increases as the number of i_{steps} increases, as shown in Figure 1. It's worth noting that even if there are zero i_{steps}, the processing time is not zero, as M_{steps} also require some time. However, the equilibration of a system with a relatively high temperature is achieved faster than a low-temperature one. The processing time scales approximately with lattice size $t \propto L^{\alpha}$, where α is the slope of each fitted line in Figure 2. The scaling exponents are above 1 for all β indicating that the processing time grows faster than a linear scaling, reflecting the increased computational cost required to handle larger systems. At lower temperatures, the processing time grows more rapidly with lattice size. While it takes less time for higher temperatures (lower β), this can be seen from the smaller γ of $\beta = 1.0$, indicating slower growth of processing time with lattice size. This behavior is due to the slower equilibration in low temperatures with more pronounced quantum effects.

From the fitting of plots of processing time (t) with simulation parameters, t scales as:

$$t(L, \beta, M_{\text{steps}}, i_{\text{steps}}) = L^{\alpha} \cdot \beta^{\gamma} \cdot M_{\text{steps}}^{\delta} \cdot 10^{B_2(\log i_{\text{steps}})^2 + B_1 \log i_{steps} + B_0}, \quad (13)$$

where, B_1, B_2 and B_0 are the polynomial coefficients from the log-log fitting of i_{steps}, and $\alpha, \gamma,$ and δ are the scaling exponents derived from the other parameters, each one of these coefficients is shown in the following figures and will be discussed individually.

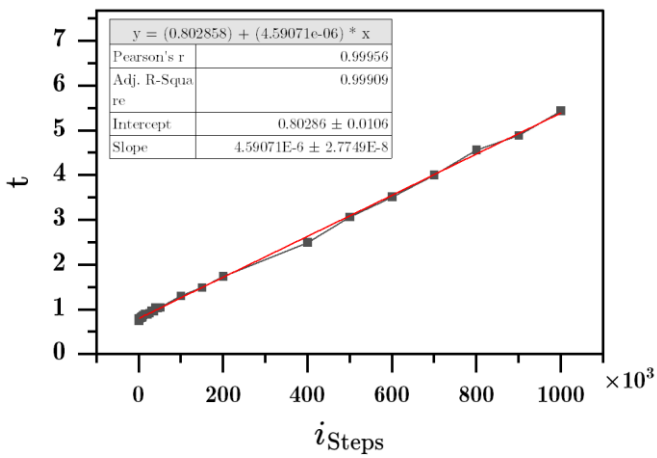

Note: Here, $L = 128, \beta = 2, M_{\text{steps}} = 7 \times 10^4$. A direct relation appears, showing the effect of i_{steps} on computational cost.

Figure 1. Relation between i_{steps} and time in seconds

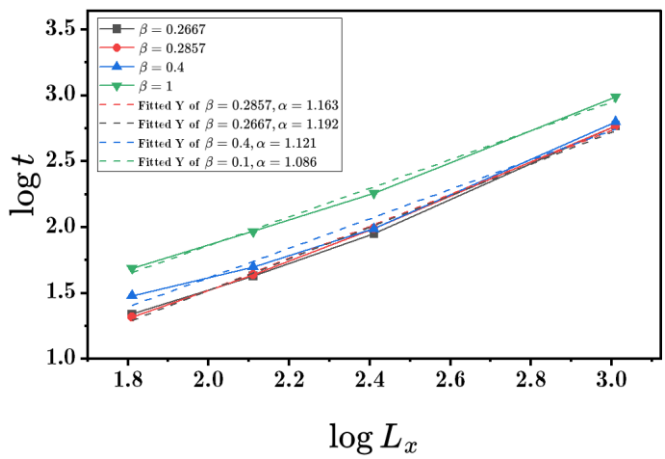

Note: The slope (α) of the fitted lines represents the scaling exponent. Each curve corresponds to a different β values.

Figure 2. Log-log plot of processing time (t) versus lattice size (L) for various values of β, with $M_{\text{steps}} = 10^6$ and $i_{\text{steps}} = 10^4$

We can see that t exhibits district scaling behavior with various simulation parameters. Figure 2 demonstrates the power law relationship between time and lattice size, where α vary slightly with β. This highlights that computational cost increases with system size due to larger configurations requiring more extensive calculations. Figure 3 presents the relationship between processing time and i_{steps}. Here we applied a second–degree polynomial fitting to capture the non-linear trend. For small values of i_{steps}, the negative linear term $(-0.285.\log i_{\text{steps}})$ leads to a decrease in the processing time, but rapid growth for larger i_{steps} is observed in the term $\left(0.06464 \cdot (\log i_{\text{steps}})^2\right)$ which causes a sharp increase in t. The nonlinear scaling underscores the importance of carefully selecting i_{steps} to balance computational cost and accuracy.

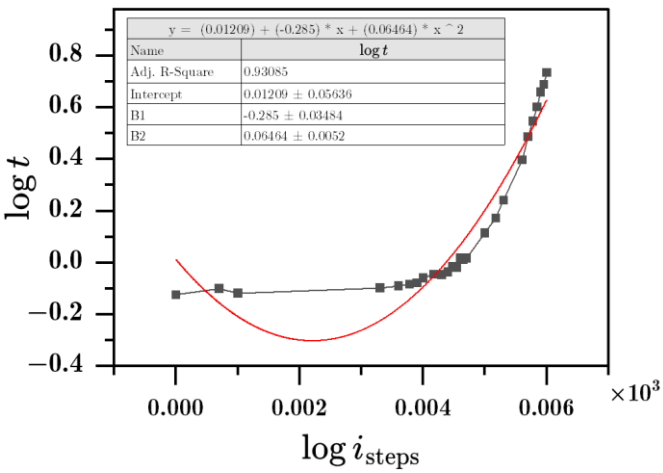

Note: The fitted equation is $\log t = 0.01209 - 0.285 \cdot \log i_{\text{steps}} + 0.06464 \cdot (\log i_{\text{steps}})^2$, indicating non-linear scaling behavior. The adjusted $R^2 = 0.93085$ demonstrates a strong fit.

Figure 3. Log-log plot of processing time versus i_{steps} with a second-degree polynomial fit

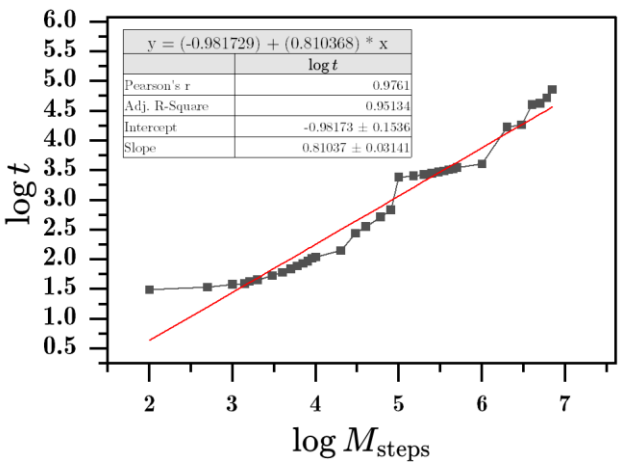

Note: The slope ($\delta = 0.81037 \pm 0.03141$) of the fitted line represents the scaling exponent. The high adjusted R^2 value (0.95134) signifies a strong linear correlation between $\log(t)$ and $\log(M_{\text{steps}})$

Figure 4. Log-log plot of processing time versus the number of M_{steps} for a fixed L, i_{steps}, β

Figure 4 shows that time scales with M_{steps} with scaling exponent $\delta = 0.81037$, indicating sublinear growth, thus reflecting the computational efficiency of averaging over repeated steps. In Figure 5, the processing time increases modestly as β increases with the scaling exponent ($\gamma = 0.565$). The inverse temperature (β) influences the level of thermal fluctuations in the system, higher β values require more computational effort to accurately sample the configuration space and achieve equilibration.

Figure 6 shows that lower temperatures (where the quantum phenomena are dominant) require longer processing time. Yet the effect of equilibration i_{steps} is obvious for lower temperatures, too. Thus 10^4 i_{steps} took 222 seconds but more than 5000 seconds were taken for 10^6 i_{steps} for the same temperature. On the other hand, the processing time of all five cases of i_{steps} was the same for higher temperatures., i.e., they required fewer equilibration steps.

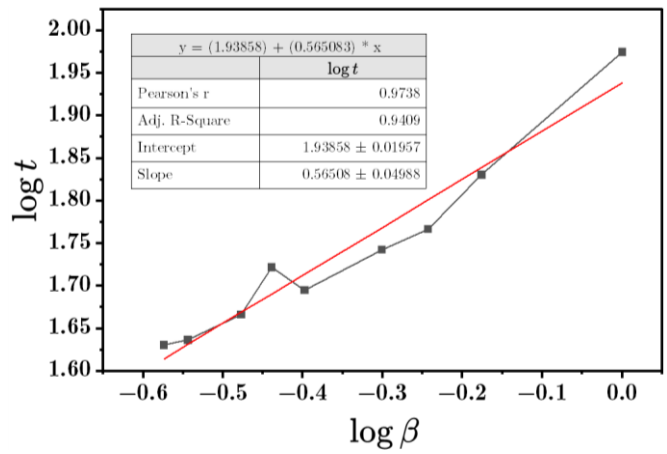

Note: The slope ($\gamma = 0.56508$) of the fitted line represents the scaling exponent. The high R^2 value (0.9409) indicates a strong linear relationship.

Figure 5. Log-log plot of processing time versus inverse temperature (β) for a lattice size $L = 128, M_{\text{steps}} = 10^6$, and $i_{\text{steps}} = 10^4$

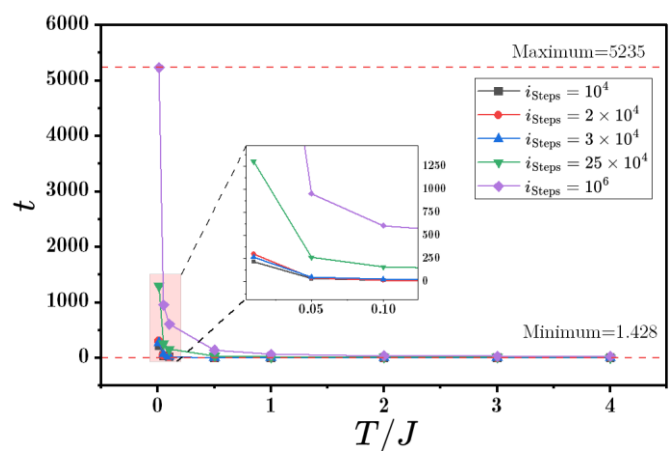

Note: Here $L = 1024, \beta = 2$, and $M_{\text{steps}} = 7 \times 10^4$. Higher temperatures require smaller processing time, however, i_{steps} effect on processing time appears in lower temperatures.

Figure 6. Processing time in seconds for a range of dimensionless temperatures, for multiple i_{steps}

3.2 Magnetic properties with different i_{steps}

We investigated the outcomes of different system properties in various temperatures and for different cases of i_{steps}. Ground state energy of quantum spin-1/2 chain increases with temperatures, as shown in Figure 7. A match of all the outcomes is noticed for all the i_{steps} cases, indicating that the

studied system's equilibration reached all i_{steps} counts, and the results were nearly the same. We can see from Table 1 that the standard deviation (σ) is larger for lower number of i_{steps}, and the results deviate from the exact solution. By using a low temperature ($\beta = 64$), the system approaches the zero-temperature limit, allowing the results to approximate the exact ground-state energy per spin calculated using the Bethe ansatz, which is defined for absolute zero temperature [27].

The magnetization shows higher values at low temperatures (see Figure 8), reflecting strong correlation between spins. As the temperature increases, thermal fluctuations dominate, leading to a gradual decrease in the property. The result is consistent across different i_{steps}, i.e., the system reaches equilibrium and is not influenced by varying i_{steps}.

The susceptibility peaks at intermediate temperatures as shown in Figure 9, representing the formation of short-range correlations. In such temperatures, the system transitions into the Curie-Weiss behavior [28, 29] due to the paramagnetic response of spins. The inset shows minor differences at low i_{steps}, but the overall trend is consistent across different equilibration steps. In the case of specific heat, Figure 10 shows that at low temperatures, smaller i_{steps} introduce greater fluctuations, indicating insufficient equilibration. As temperature increases, C aligns across all i_{steps}. At $T/J = 0.5$, the specific heat reflects the Schottky-like anomaly, associated with thermal excitations between spin states. At higher temperatures, C approaches a constant value, reflecting equipartition.

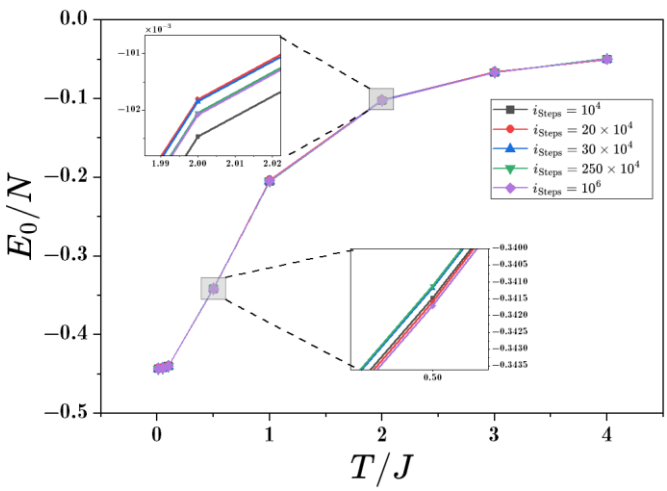

Note: Here $L = 1024$, and $M_{\text{steps}} = 10^4$. Energy increases as temperature increases. All of i_{steps} results are nearly the same.

Figure 7. Ground state energy relation with the dimensionless temperature at a range of i_{steps}

In Table 1, the lattice size $L = 128$, $\beta = 1/64$, and $M_{\text{steps}} = 10^4$. Insufficient i_{steps} lead to results that have a larger σ and deviate from the exact solution obtained via Beth Ansatz.

Table 1. Standard deviation (σ) of energy results for various i_{steps}, calculated with $N_{\text{bins}} = 10$

i_{steps}	$\sigma_{E_0/N}$	$\sigma_{\text{from exact}}$
10	0.197682899	0.319404056
10^4	0.050776845	0.000128659
10^5	0.050906944	0.000101979

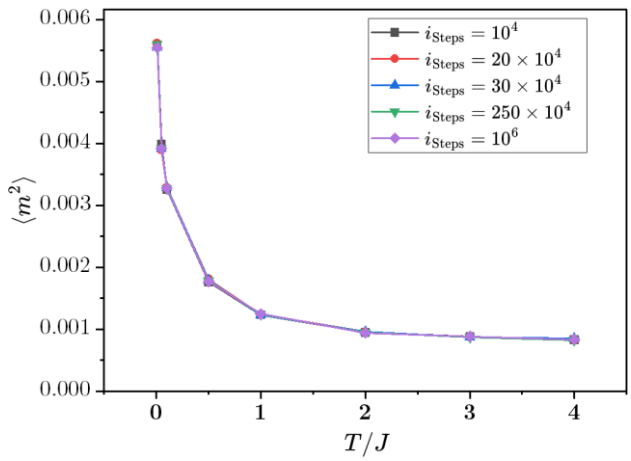

Note: Where L = 1024, and $M_{\text{steps}} = 10^4$. No noticeable variance in the results appears.

Figure 8. The relation between sublattice magnetization and dimensionless temperatures, each point simulated in multiple counts of i_{steps}

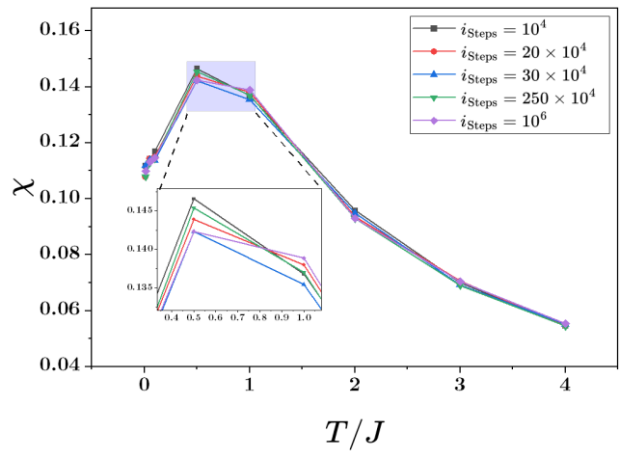

Note: Where $L = 1024$, and $M_{\text{steps}} = 10^4$.The results for higher and lower temperatures match all the i_{steps} counts. The inset figure shows a minor deviation between 0.5 and 1 temperature.

Figure 9. Susceptibility versus dimensionless temperature for different i_{steps} counts

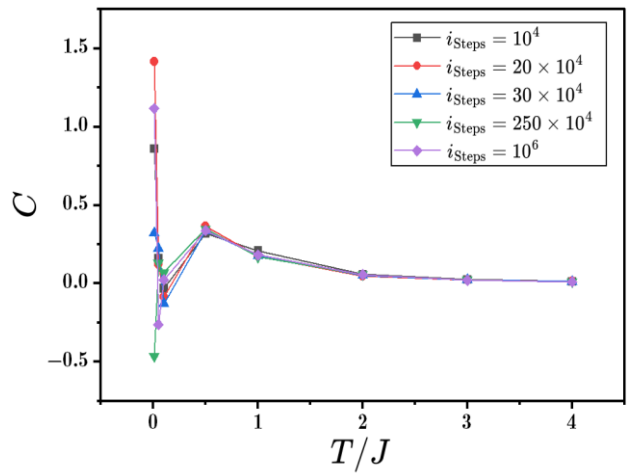

Note: System size is $L = 1024$, with and M_{steps} 10^4. No matter how the i_{step} increases, lower temperatures show less convergence of results. However, the results of higher temperatures for specific heat are the same.

Figure 10. Specific heat for a range of dimensionless temperatures and various i_{steps}

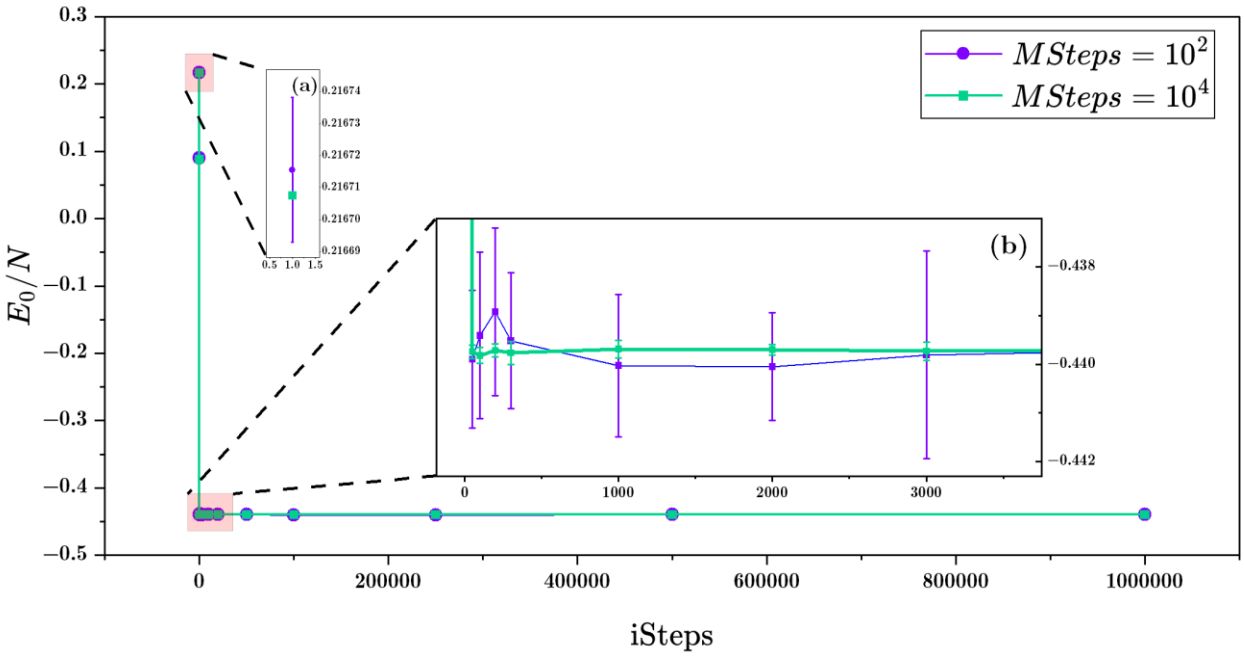

Note: Accurate results were achieved after 50 i_{steps}, and they continued to give similar results. The error bars show that more M_{steps} reduce errors.

Figure 11. Ground state energy measurements with various i_{steps}, for two numbers of M_{steps}, $L = 1024, \beta = 0.1, N_{\text{Bins}} = 10$

Table 2. Statistical analysis of observables as a function of i_{steps}

Observable	i_{steps}	$\langle X \rangle$	σ	σ^2	$\frac{\sigma}{\langle X \rangle}$
$\frac{E_0}{N}$	10	-1.78003E-01	3.82E-04	1.46E-07	-2.15E-03
	10^4	-3.41552E-01	9.26E-04	8.58E-07	-2.71E-03
	5×10^4	-3.41433E-01	6.58E-04	4.33E-07	-1.93E-03
	10^5	-3.41338E-01	6.37E-04	4.05E-07	-1.87E-03
	5×10^5	-3.41336E-01	4.53E-04	2.05E-07	-1.33E-03
	10^6	-3.41372E-01	7.83E-04	6.12E-07	-2.29E-03
C	10	-7.53187E-01	4.90E-03	2.40E-05	-6.50E-03
	10^4	3.49410E-01	2.88E-02	8.31E-04	8.25E-02
	5×10^4	3.38704E-01	2.30E-02	5.29E-04	6.79E-02
	10^5	3.44273E-01	3.39E-02	1.15E-03	9.84E-02
	5×10^5	3.47675E-01	2.57E-02	6.61E-04	7.40E-02
	10^6	3.50791E-01	2.77E-02	7.69E-04	7.91E-02
$\langle m^2 \rangle$	10	1.26380E-02	1.86E-04	3.45E-08	1.47E-02
	10^4	1.43949E-02	9.70E-05	9.46E-09	6.76E-03
	5×10^4	1.43729E-02	7.70E-05	6.00E-09	5.39E-03
	10^5	1.43487E-02	1.29E-04	1.66E-08	8.99E-03
	5×10^5	1.43276E-02	2.41E-04	5.80E-08	1.68E-02
	10^6	1.43938E-02	1.49E-04	2.22E-08	1.04E-02
χ	10	1.87244E-01	3.33E-03	1.11E-05	1.78E-02
	10^4	1.42351E-01	1.90E-03	3.59E-06	1.33E-02
	5×10^4	1.43882E-01	1.20E-03	1.44E-06	8.34E-03
	10^5	1.44040E-01	1.96E-03	3.84E-06	1.36E-02
	5×10^5	1.43861E-01	2.01E-03	4.04E-06	1.40E-02
	10^6	1.42515E-01	2.10E-03	4.43E-06	1.48E-02

Table 2 lists the average values $\langle X \rangle$, standard deviation (σ), variance (σ^2), and relative deviation $(\sigma/\langle X \rangle)$ for each observable. The results demonstrate that i_{steps} does not significantly influence the convergence of data across multiple simulation runs, as evidenced by the relatively constant standard deviation and variance.

3.3 Results accuracy and convergence

Measurements in the SSE method are taken after the equilibration is reached. Several i_{steps} are used for this purpose. However, those steps take time, as discussed above. A threshold of i_{steps} can be calculated for the system of investigation where the results remain similar regardless of the number of i_{steps} added; Figure 11 shows that insufficient i_{steps} count gives inaccurate outcomes as in the incent Figure 11(a), the energy in the first two points of the data doesn't represent the actual value of the system. Conversely, more elevated i_{steps} give the same results; Higher M_{steps} count reduces error bars as appears in Figure 11(b). The data in Table 2 clearly show that i_{steps} does not govern the convergence of the results from multiple runs of simulation, as σ and σ^2 remains largely

unchanged across different i_{steps}. This also indicates that the convergence of data is the responsibility of M_{steps} which ensures proper sampling and reduces variability across runs. Nevertheless, i_{steps} is crucial for the accuracy of results. Proper i_{steps} ensures that the system is equilibrated and the measurements reflect the true magnetic behavior of the system. This highlights the roles of M_{steps} and i_{steps} in achieving both convergence and accuracy in the simulation data.

We represent from Figures 12-15 a repeated simulation results for the same conditions and two different values of i_{steps} to assess the reliability and consistency of the simulation outcomes. These figures highlight the impact of varying i_{steps} under extreme temperature, both very high and very low, on the studied magnetic properties.

In Figure 12, E_0/N demonstrates consistent results across 40 simulation runs for both low and high temperatures. However, at low i_{steps} (Figure 12(a)) the energy values for high and low temperatures appear nearly identical, suggesting that the system has not yet reached equilibrium. But the higher i_{steps} in Figure 12(b), the high temperature simulations yield higher energy values as expected from real magnetic system, indicating improved precision.

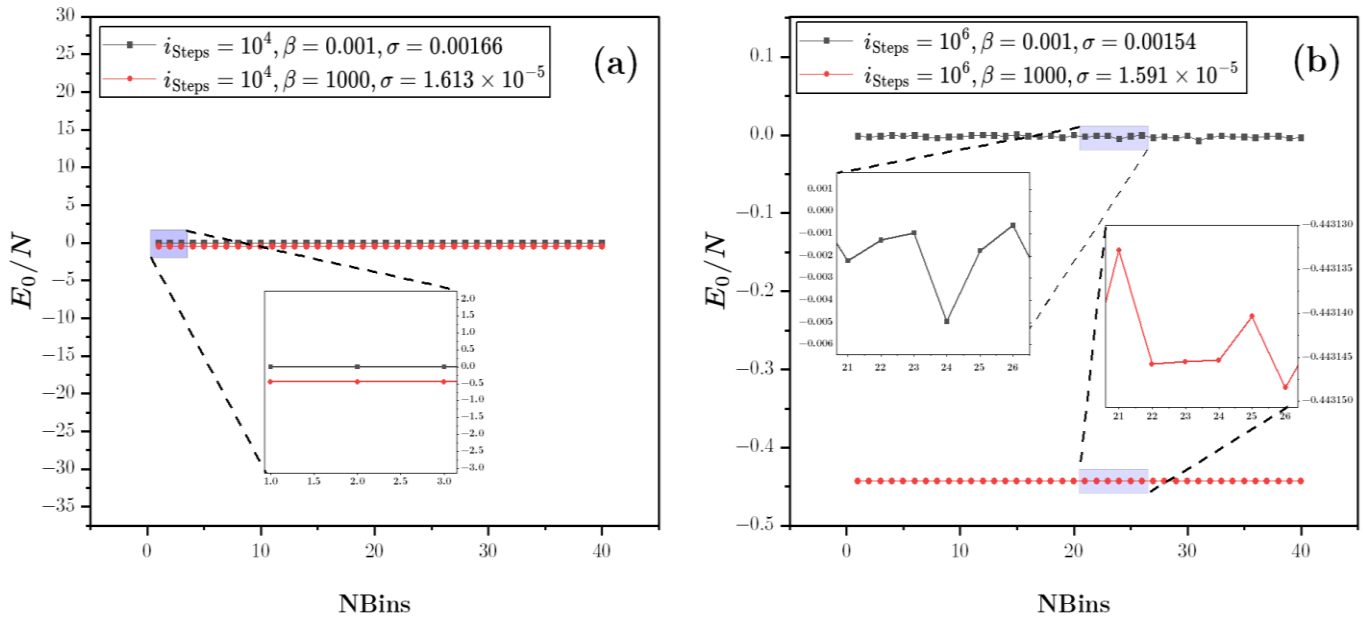

Figure 12. Results of energy for 40 runs of the same simulation for low and high temperatures with (a) 10^4 and (b) 10^6 i_{steps}, where $L = 1024$, and $M_{\text{steps}} = 10^4$

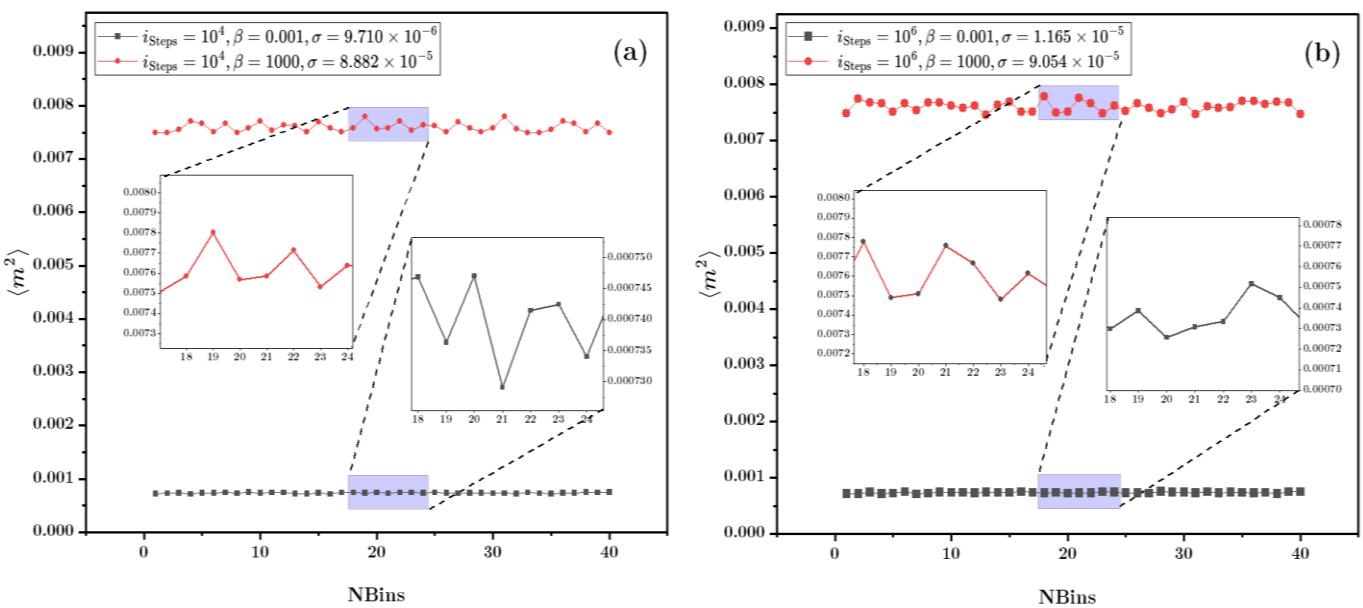

Note: The property has a reverse relation with temperature. And it converges more for higher temperatures.

Figure 13. Simulation outcomes of sublattice magnetization for low and high temperatures for a system with $L = 1024$ spin sites. Each NBin results from averaging 10^4 M_{steps}, after equilibrating the system by (a) 10^4 and (b) 10^6 i_{steps}

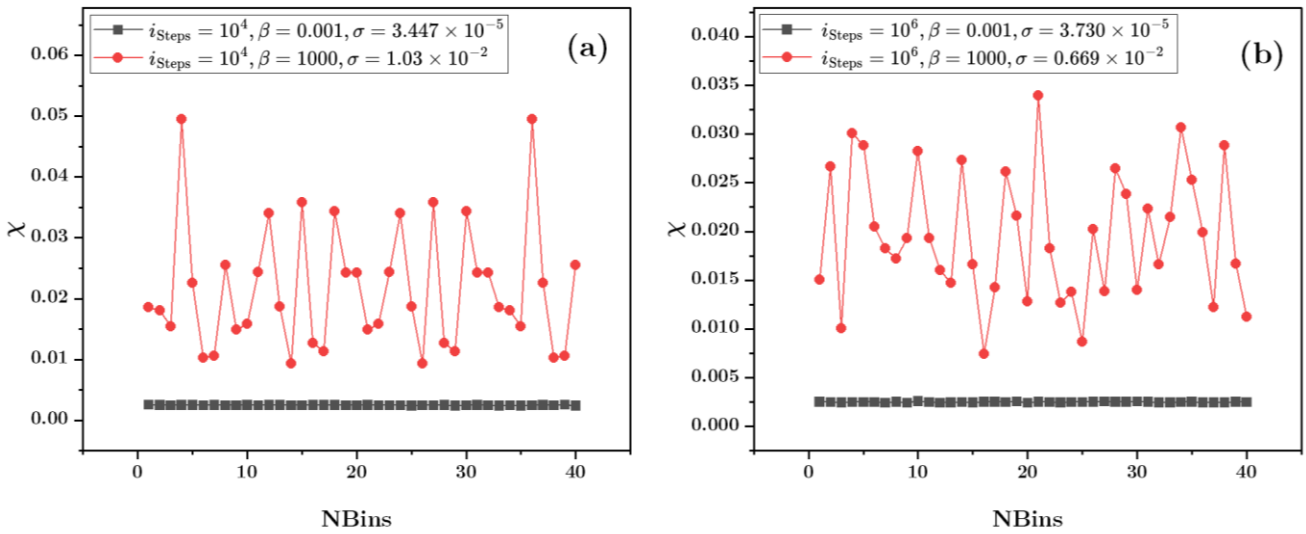

Note: Results of higher temperatures shows less standard deviation σ.

Figure 14. Susceptibility results for 40 N_{Bins}, for system size $L = 1024$, at each point, susceptibility was measured by averaging the results of 10^4 M_{steps}after (a) 10^4 and (b) 10^6 equilibration Monte Carlo steps

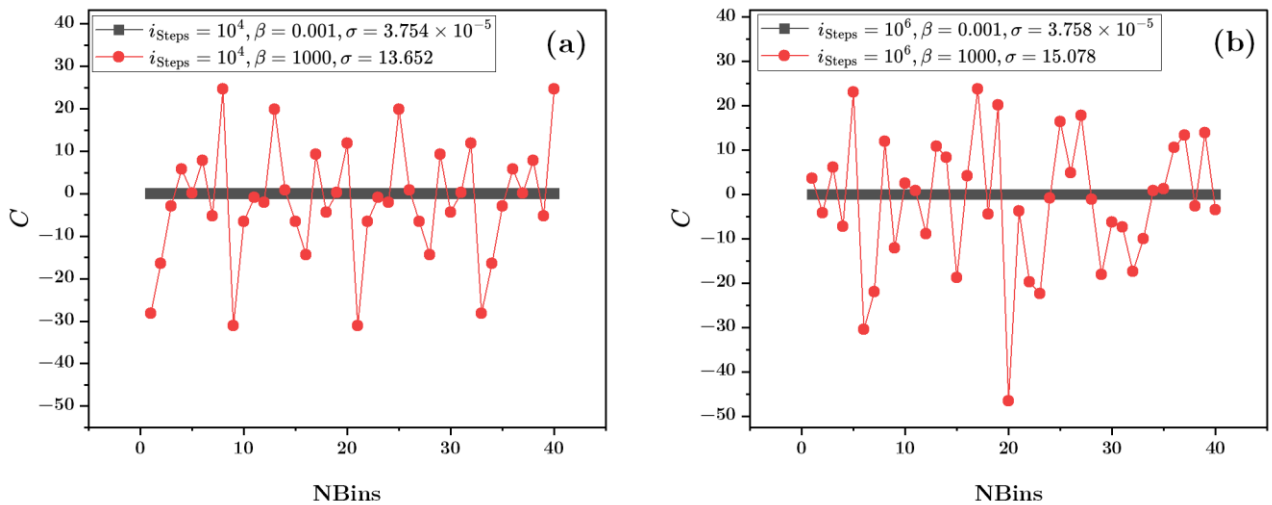

Note: Lower temperatures (i.e. higher β) show major fluctuations of results.

Figure 15. Specific heat of $L = 1024$, where $M_{\text{steps}} = 10^4$, each point represents on run of simulation at low and high temperatures, the i_{steps} was (a) 10^4 and (b) 10^6

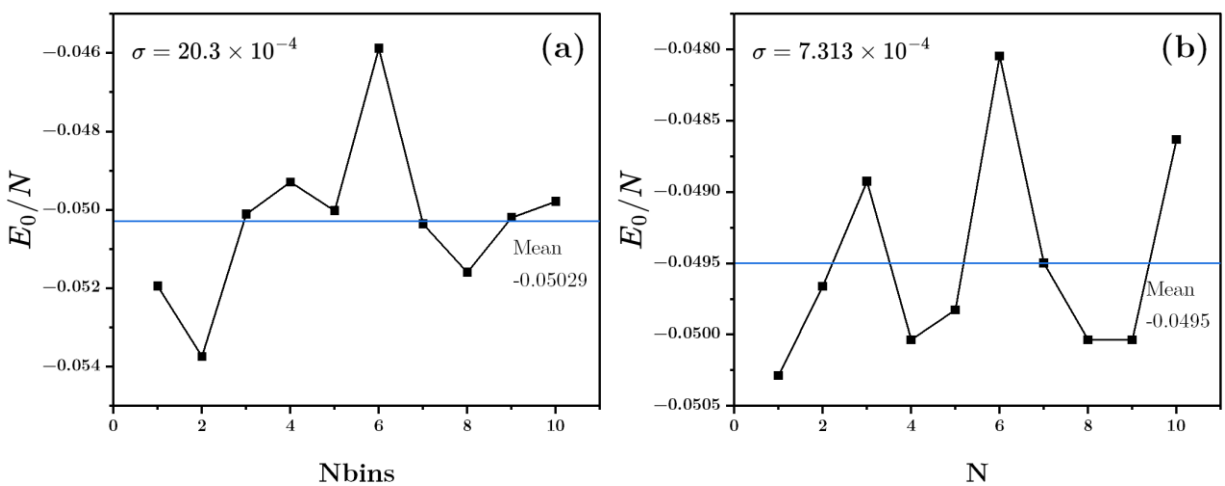

Note: A noticeable decrease in σ value for higher N_{Bins} simulation.

Figure 16. Repeating the simulation of the same conditions where $L = 64, \beta = 0.25$, and $M_{\text{steps}} = i_{\text{steps}} v = 10^4$, each point in the figure represents (a) 1 and (b) 10 N_{Bins}

$\langle m^2 \rangle$ shows higher values and larger standard deviations at lower temperatures (see Figure 13), consistent with the expected stronger ordering in the system. Figure 13(a) and (b) both display reliable results across repeated simulations, thus increase in the i_{steps} does not significantly affect the outcomes. The results of specific heat and susceptibility, shown in Figure 14 and Figure 15, exhibit more pronounced temperature dependence. At low temperature, the red data points in Figure 14(a) and (b) oscillate within a wider range (0.01 to 0.05 for χ), reflecting the challenge of achieving precise convergent in this regime. Higher temperature simulations (black data points) remain relatively stable, with minimal influence from i_{steps}. Similar for C, low-temperature results show significant fluctuations, while high temperatures yield consistent outcomes (Figure 15). We can notice that increasing i_{steps} from 10^4 to 10^6 does not significantly alter the results for C, thus the convergence for this property is not governed by i_{steps}. Figure 16 demonstrates the effect of averaging over multiple bins on the stability and reliability of the simulation results for the ground state energy per spin, where $N_{bins} = 10$ in Figure 16(a), the data shows a higher standard deviation ($\sigma = 20.3 \times 10^{-4}$), By increasing the N_{bins} to 100 (see Figure 16(b)), σ significantly decreases to 7.31×10^{-4}, reflecting a more stable and consistent set of results. The reduced variability for higher N_{bins} ensures greater confidence in the accuracy of the reporter results.

3.4 Criteria for determining appropriate i_{steps}

The accuracy and stability of SSE simulations are contingent upon selecting an adequate number of equilibration steps (i_{steps}) . We outline a systematic frame work for determining the optimal i_{steps}.

1. Preliminary Investigations:

Initial trail simulations should be conducted across a range of i_{steps} to identify the equilibration threshold. Key observables, such as E_0/N and $\langle m^2 \rangle$ should be monitored for evidence of stabilization. If a plateau appears in these observables, then the system has reached equilibrium.

2. Autocorrelation Analysis:

The auto correlation time of critical observables provides a quantitative measure of the statistical independence between successive configurations. i_{steps} should must exceed the auto correlation time by a factor at least 10.

3. Statistical Validation:

To ensure robust equilibration, the stability of statistical measures such as the mean and variance of observables should be evaluated. Convergence is achieved when the mean value stabilizes within a predefined tolerance and the variance exhibits no significant dependence on i_{steps}.

It is noted that higher temperatures may diminish the requisite number of i_{steps} for equilibration, whereas larger systems typically necessitate an increased number of i_{steps}. Statistical methods should be employed to ascertain the stabilization of the mean and variance of the measurements, thereby ensuring robust and reliable simulation outcomes.

4. STUDY LIMITATIONS

This study provides valuable insights into the impact of i_{steps} on the accuracy, stability, and computational cost of SSE simulations. However, several limitations should be noted:

- The simulations were limited to relatively small system sizes. While these sizes are sufficient to demonstrate key trends and validate the methodology, larger systems could reveal additional scaling effects and subtleties in the behavior of magnetic properties.
- The analysis was confined to a one-dimensional system. Extending this approach to higher-dimensional systems (e.g., 2D or ladder geometries) could provide a more comprehensive understanding of the impact of i_{steps} , under varying coordination numbers and dimensionalities.
- The simulations were conducted on a single workstation with fixed hardware specifications. Parallelization strategies or simulations on more advanced computing clusters could provide deeper insights, particularly for larger systems or higher-dimensional models.

5. CONCLUSION

This study examines the role of equilibration steps in the SSE method for simulating the 1D spin-1/2 antiferromagnetic lattice defined by the Heisenberg model. The findings highlight the critical importance of equilibration steps in achieving stable and reliable simulation outcomes while balancing computational cost. The analysis demonstrates that ground state energy per spin and sublattice magnetization remain stable across different equilibration step counts, particularly at low temperatures, closely matching the exact Bethe ansatz solution. In contrast, susceptibility and specific heat show variability at low temperatures due to dominant quantum effects. At intermediate temperatures, susceptibility peaks reflect the formation of short-range spin correlations and transition into Curie-Weiss behavior at high temperatures. The results also emphasize that increasing the number of bins significantly enhances result stability by reducing statistical deviations.

Equilibration steps are vital to ensure accurate representation of the system's equilibrium properties, particularly at low temperatures where slower equilibration leads to greater fluctuations. Measurement steps, on the other hand, govern the convergence of results across multiple runs, ensuring proper sampling and consistency.

Future work could explore these findings in higher-dimensional systems, ladder geometries, or more complex spin interactions. An automated algorithm could be developed to optimize simulation parameters, such as equilibration and measurement steps, based on the system's properties, including lattice size and temperature. The algorithm would perform several preliminary runs to analyze the system's behavior and identify the optimal values for equilibration and measurement steps that ensure both accuracy and computational efficiency. Additionally, the algorithm could factor in the hardware specifications of the system it is running on, such as the processor type, available RAM, and computational power. The algorithm could adapt to hardware capabilities, efficiently allocating resources and recommending parameters that balance accuracy and runtime. This automation would save time, especially for larger lattices or low temperatures, reducing trial-and-error and enabling researchers to focus on analyzing results.

REFERENCES

[1] Giudici, G., Mendes-Santos, T., Calabrese, P., Dalmonte, M. (2018). Entanglement Hamiltonians of lattice models via the Bisognano-Wichmann theorem. Physical Review B, 98(13): 134403. https://doi.org/10.1103/PhysRevB.98.134403

[2] Tarasov, V. (2018). Completeness of the Bethe ansatz for the periodic isotropic Heisenberg model. Reviews in Mathematical Physics, 30(8): 1840018. https://doi.org/10.1142/S0129055X18400184

[3] Schubert, D., Richter, J., Jin, F., Michielsen, K., De Raedt, H., Steinigeweg, R. (2021). Quantum versus classical dynamics in spin models: Chains, ladders, and square lattices. Physical Review B, 104(5): 054415. https://doi.org/10.1103/PHYSREVB.104.054415/FIGURES/7/THUMBNAIL

[4] Yang, C.N., Yang, C.P. (1966). One-dimensional chain of anisotropic spin-spin interactions. I. Proof of Bethe's hypothesis for ground state in a finite system. Physical Review, 150(1): 321-327. https://doi.org/10.1103/PhysRev.150.321

[5] Merali, E., De Vlugt, I.J., Melko, R.G. (2024). Stochastic series expansion quantum Monte Carlo for Rydberg arrays. SciPost Physics Core, 7(2): 016. https://doi.org/10.21468/SciPostPhysCore.7.2.016

[6] Dorneich, A., Troyer, M. (2001). Accessing the dynamics of large many-particle systems using the stochastic series expansion. Physical Review E, 64(6): 066701. https://doi.org/10.1103/PhysRevE.64.066701

[7] Kawaki, K., Kuno, Y., Ichinose, I. (2017). Phase diagrams of the extended Bose-Hubbard model in one dimension by Monte-Carlo simulation with the help of a stochastic-series expansion. Physical Review B, 95(19): 195101. https://doi.org/10.1103/PHYSREVB.95.195101/FIGURES/13/MEDIUM

[8] Pavarini, E. (2019). Many-body methods for real materials lecture notes of the Autumn School on Correlated Electrons 2019. Beijing, China: Forschungszentrum Jülich GmbH Institute of Advanced Simulation. https://www.cond-mat.de/events/correl19/manuscripts/correl19.pdf.

[9] Wang, L., Liu, Y.H., Troyer, M. (2016). Stochastic series expansion simulation of the *t*-*V* model. Physical Review B, 93(15): 155117. https://doi.org/10.1103/PhysRevB.93.155117

[10] Sandvik, A.W. (2010). Computational studies of quantum spin systems. AIP Conference Proceedings, 1297(1): 135-338. https://doi.org/10.1063/1.3518900

[11] Feynman, R.P. (1953). Atomic theory of the λ transition in Helium. Physical Review, 91(6): 1291-1301. https://doi.org/10.1103/PhysRev.91.1291

[12] Assaad, F.F., Lang, T.C. (2007). Diagrammatic determinantal quantum Monte Carlo methods: Projective schemes and applications to the Hubbard-Holstein model. Physical Review B—Condensed Matter and Materials Physics, 76(3): 035116. https://doi.org/10.1103/PhysRevB.76.035116

[13] Hirsch, J.E., Sugar, R.L., Scalapino, D.J., Blankenbecler, R. (1982). Monte Carlo simulations of one-dimensional fermion systems. Physical Review B, 26(9): 5033-5055. https://doi.org/10.1103/PhysRevB.26.5033

[14] Sandvik, A.W., Kurkijärvi, J. (1991). Quantum Monte Carlo simulation method for spin systems. Physical Review B, 43(7): 5950-5961. https://doi.org/10.1103/PhysRevB.43.5950

[15] Suzuki, M. (1976). Relationship between *d*-dimensional quantal spin systems and (*d*+1)-dimensional ising systems: Equivalence, critical exponents and systematic approximants of the partition function and spin correlations. Progress of Theoretical Physics, 56(5): 1454-1469. https://doi.org/10.1143/PTP.56.1454

[16] Suzuki, M. (1986). Quantum statistical Monte Carlo methods and applications to spin systems. Journal of Statistical Physics, 43: 883-909. https://doi.org/10.1007/BF02628318

[17] Syljuåsen, O.F., Sandvik, A.W. (2002). Quantum Monte Carlo with directed loops. Physical Review E, 66(4): 046701. https://doi.org/10.1103/PhysRevE.66.046701

[18] Prokof'ev, N.V., Svistunov, B.V., Tupitsyn, I.S. (1996). Exact quantum Monte Carlo process for the statistics of discrete systems. Journal of Experimental and Theoretical Physics Letters, 64: 911-916. https://doi.org/10.1134/1.567243

[19] Sandvik, A.W. (1997). An introduction to quantum monte carlo methods. In: Sierra, G., Martín-Delgado, M.A. (eds) Strongly Correlated Magnetic and Superconducting Systems. Lecture Notes in Physics, vol 478. Springer, Berlin, Heidelberg. https://doi.org/10.1007/BFb0104635

[20] Desai, N., Pujari, S. (2021). Resummation-based quantum Monte Carlo for quantum paramagnetic phases. Physical Review B, 104(6): L060406. https://doi.org/10.1103/PhysRevB.104.L060406

[21] Laflorencie, N., Rieger, H., Sandvik, A.W., Henelius, P. (2004). Crossover effects in the random-exchange spin-$\frac{1}{2}$ antiferromagnetic chain. Physical Review B—Condensed Matter and Materials Physics, 70(5): 054430. https://doi.org/10.1103/PhysRevB.70.054430

[22] Kargarian, M., Jafari, R., Langari, A. (2008). Renormalization of entanglement in the anisotropic Heisenberg (*XXZ*) model. Physical Review A—Atomic, Molecular, and Optical Physics, 77(3): 032346. https://doi.org/10.1103/PhysRevA.77.032346

[23] Sandvik, A.W. (1997). Finite-size scaling of the ground-state parameters of the two-dimensional Heisenberg model. Physical Review B, 56(18): 11678-11690. https://doi.org/10.1103/PhysRevB.56.11678

[24] Margraf, D., Cekan, P., Prisner, T.F., Sigurdsson, S.T., Schiemann, O. (2009). Ferro-and antiferromagnetic exchange coupling constants in PELDOR spectra. Physical Chemistry Chemical Physics, 11(31): 6708-6714. https://doi.org/10.1039/B905524J

[25] Handscomb, D.C. (2008). A Monte Carlo method applied to the Heisenberg ferromagnet. Mathematical Proceedings of the Cambridge Philosophical Society, 60(1): 115-122. https://doi.org/10.1017/S030500410003752X

[26] Sandvik, A.W., Evertz, H.G. (2010). Loop updates for variational and projector quantum Monte Carlo simulations in the valence-bond basis. Physical Review B—Condensed Matter and Materials Physics, 82(2): 024407. https://doi.org/10.1103/PhysRevB.82.024407

[27] Parkinson, J.B., Farnell, D.J.J. (2010). The antiferromagnetic ground state. An Introduction to Quantum Spin Systems, 39-47. https://doi.org/10.1007/978-3-642-13290-2_4

[28] Niraula, G., Wu, C., Yu, X., Malik, S., Verma, D.S., Yang, R., Zhao, B., Ding, S., Zhang, W., Sharma, S.K. (2024). The Curie temperature: A key playmaker in self-regulated temperature hyperthermia. Journal of Materials Chemistry B, 12(2): 286-331. https://doi.org/10.1039/D3TB01437A

[29] Curie, P. (2018). Propriétés Magnétiques des Corps à Diverses Températures (Classic Reprint). Forgotten Books.

NOMENCLATURE

$\langle \hat{A} \rangle$	Thermal expectation value
$\hat{S}^+, \hat{S}^-$	Raising and lowering spin operators
$\langle \mathrm{X} \rangle$	Average
E_0/N	Ground state energy per spin, J
$\hat{H}$	Hamiltonian
M_{steps}	Measurement Monte Carlo steps
N_{Bins}	Number of bins
N_b	Number of bonds
i_{steps}	Equilibration Monte Carlo steps
m	Dimensionless sublattice magnetization
h	External magnetic fields
B	Polynomial coefficient
C	Specific heat
L	Lattice size
N	The number of sites in the lattice equals
T	Absolute temperature, K
W	Weight of configuration
Z	Partition function
c	Constant number
t	Processing time
z	Z-direction
χ	Susceptibility, $\mathrm{J/T^2}$
ϵ	Proportionality constant

Greek symbols

α	scaling exponent of t with L
β	inverse dimensionless temperature
γ	scaling exponent of t with β
δ	scaling exponent of t with M_{steps}
$\lvert\varphi\rangle$	basis state of the system
σ	Standard Deviation
Δ	uniaxial anisotropy